



Investigating structure-charge transport relationships in thiophene substituted naphthyridine crystalline materials by computational model systems

Received 00th January 20xx,
Accepted 00th January 20xx

DOI: 10.1039/x0xx00000x

www.rsc.org/

Madeline M. Lewis, Adeel A. Ahmed, Lisa Gerstmann and Jesus Calvo-Castro*

The development of novel π -conjugated charge transfer mediators is at the forefront of current research efforts and interests. Among the plethora of building blocks, diketopyrrolopyrroles have been widely employed, associated to the ease of tailoring their optoelectronic properties by systematic peripheral substitutions. It is somehow of surprise to us that their six-member ring bis-lactam analogues, naphthyridines have been overlooked and reports are scarce and almost solely limited to their use in polymeric materials. Herein we report a comprehensive theoretical analysis of the charge transfer properties of 1,5-naphthyridine-based materials by means of a number of bespoke model systems, further able to quantitatively predict experimental mobility observations. Our results imply that thiophene substituted naphthyridine crystalline materials represent a promising class of organic π -conjugated systems with an experimentally observed ability to self-assemble in the solid state conforming to one dimensional stacking motifs. These highly sought-after charge propagation channels are characterised by large wavefunction overlap and thermal integrity and have as a result the potential to outperform currently exploited alternatives. We anticipate this work to be of interest to materials scientists and hope it will pave the way towards the realisation of novel charge transfer mediators exploiting naphthyridine chemistries.

Introduction

Largely aided by improvements in material design and purification, over the last two decades there have been major advances in the development of organic systems that can be exploited as charge transfer mediating materials in optoelectronic applications.^{1–4} To facilitate their translation into applications that can be exploited commercially, most reported charge mobility measurements in the literature refer to their performance in crystalline and amorphous thin film architectures. However, by limiting the evaluation of novel materials to observations in thin film architectures, potentially good performers can be often overlooked on the basis of poor preliminary results which can be ascribed to device architecture and not the intrinsic properties of the materials.² As a result, organic single crystals denote an ideal platform in realising the effective performance in optoelectronic devices in light of their superior purity and longer-range order when compared against their thin film counterparts.^{4–6}

Along those lines, *in-silico* approaches, which can shed light into the mechanistic understanding of observed performances, identify structure-activity causations and further guide the rational

development of potentially superior alternatives by crystal engineering, are considered to be of paramount importance.^{1,7,8} Although the exact mechanism responsible for the observed mobilities in organic materials is still a matter of significant debate, particularly in the case of observed large mobilities, it is widely acknowledged that one-dimensional π - π stacking motifs represent desirable charge propagation channels for the realisation of effective charge transfer phenomenon.^{1,2} In such highly sought-after supramolecular arrangements, the relative displacements of the monomers within the stacking motif(s), specifically in relation to their long (roll) and short (pitch) axes shifts, are known to play a critical role. In fact, the switching of the nature of hole/electron mobility by small ($< 1 \text{ \AA}$) intermonomer displacements has been theoretically predicted.^{7,9–12} In addition, and contrary to previous misconceptions,¹³ it is nowadays commonly acknowledged that materials characterised by relatively large displacements along the short molecular axis (pitch angle) should not be discarded solely on that basis and, in fact, have furthermore the potential to outperform others which are more closely aligned.^{10,14} The latter highlights the relevance of wavefunction, and not simply structural overlap in the design of organic charge transfer mediators.

In developing novel small organic π -conjugated charge transfer mediating materials, two main approaches can be considered. Firstly, the often-exploited approach of performing peripheral substitution on core motifs for which successful properties have been experimentally determined, with views to induce changes in their

School of Life and Medical Sciences, University of Hertfordshire, Hatfield, AL10 9AB, UK.

Electronic Supplementary Information (ESI) available. See DOI: 10.1039/x0xx00000x

supramolecular packing arrangements that would have an effect in their charge transfer properties. Whilst some cores motifs are prone to exhibiting this behaviour,^{7,10} this has not been the case for rubrene,^{9,15} arguably the best organic charge transfer mediating material to date.^{1,5} In fact, it has been observed that in most cases, substitutions performed on rubrene's tetracene core as well as peripheral rings, result in negligible changes to the supramolecular packing motifs.⁹

On the other hand, the development of materials that have the potential to outperform currently available systems by conforming to desirable charge propagation channels in the solid state whilst exploiting novel core motifs is at the forefront of current research efforts.^{1,2} Among the plethora of organic π -conjugated core motifs employed to date, diketopyrrolopyrroles, which were first exploited as high performance pigments,^{16–18} have more recently shown promise as charge transfer mediators in account of their highly planar structure as well as the ease of tailoring their optoelectronic properties by means of peripheral substitutions on the core rings as well as lactam nitrogen atoms.^{13,16} In this regard, we have previously reported that in systems exploiting this bis-lactam unit, structural control resulting in supramolecular architectures that conform to one and two-dimensional stacking motifs can be influenced via judicious selection of substitutions.^{14,19–22}

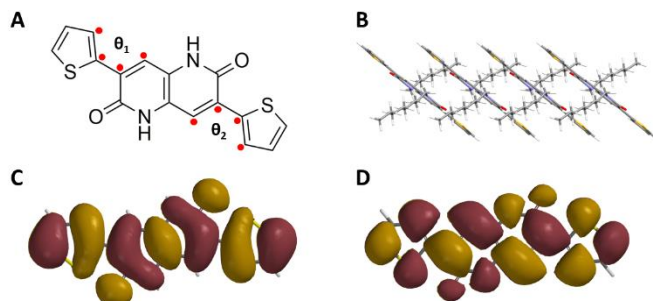


Figure 1. **A** Chemical structure of 3,7-di(thiophen-2-yl)-1,5-dihydro-1,5-naphthyridine-2,6-dione, **NTDT**. Red filled circles illustrate the dihedral angles, θ_1 and θ_2 . **B** Tetramer illustrating the one-dimensional slipped cofacial π - π stacking motif in the reported crystal structure,²³ viewed along the a crystallographic axis. **C** HOMO (**D**) wavefunctions for the model **NTDT** system, M06-2X/6-311G(d).

In light of these findings, it was somehow of surprise to us that studies investigating the charge transfer properties of the six-member ring bis-lactam analogue are scarce and almost solely limited to polymeric materials and not small molecules,^{23,24} despite their synthesis being first reported in 1971.²⁵ On searching the Cambridge Structural Database for 1,5-naphthyridine-2,6-diones (**NTDT**), only one reported structure was returned,²³ exhibiting a supramolecular arrangement whereby monomers conform to a one-dimensional supramolecular π - π stacking motifs along the *b* crystallographic axis with relatively small measured intermonomer displacements for the long ($\Delta x = 4.39 \text{ \AA}$) and short ($\Delta y = 0.79 \text{ \AA}$) molecular axes (Figure 2B).

Herein, motivated by these findings and to pave the way for the judicious realisation of superior alternatives exploiting naphthyridine chemistries, we report a comprehensive theoretical evaluation of their charge transfer properties by means of state-of-the-art **NTDT** model systems that highlight the potential of naphthyridines for making a new generation of charge transfer mediating materials and would furthermore facilitate the evaluation of novel materials. To

the best of our knowledge, this is the first study of this sort, which further includes a comprehensive analysis of the effect of commonly used density functionals and basis sets on critical charge transfer parameters.

In the hopping high-temperature regime for charge transport processes and within the semi-classical Marcus formalism,^{26–28} rate constants for hole/electron transport decrease as the inner-sphere reorganisation energy ($\lambda_{h/e}$) increases. Thus, the development of materials characterised by small structural re-arrangements on progression from neutral to radical geometries is highly warranted. As a result, the first part of this work is devoted to the careful analysis of computed $\lambda_{h/e}$, of both optimised geometries as well as model systems whereby the effect of simultaneous thiophene ring torsion in the parent **NTDT** is evaluated in depth. Our findings highlight that **NTDT** based systems are characterised by $\lambda_e > \lambda_h$, with λ_h exhibiting negligible changes as a function of core ring torsion as a result of counteracting structural re-arrangements. Subsequently, the study focuses on the evaluation of transfer integrals by means of bespoke dimeric model system which confirm negligible changes in computed $t_{h/e}$ employing different basis sets and density functionals. Contrary to popular misconceptions, we report that remarkably large $t_{h/e}$ are anticipated for one-dimensional stacks whereby short molecular axis intermonomer displacements are significant. Hence expanding the plethora of supramolecular packing motifs with superior predicted properties to those currently existing. Lastly, we evaluated the thermal integrity of these dimeric units by computing their intermolecular interactions. Importantly, we report that the utilisation of basis sets larger than 6-311G(d) result in negligible changes in the computed ΔE_{CP} despite their significantly larger computational cost. By means of two-dimensional models we highlight the **NTDT** systems are intrinsically characterised by large ΔE_{CP} which can be rationalised based on the synergistic effect of relatively weak dipole-dipole and induced dipole intermolecular interactions. In all cases, our developed model systems were observed to account well for theoretical and experimental parameters determined for the reported crystal structure and as such we anticipate this work to be of interest to the increasingly large multidisciplinary community of materials scientists devoted to the development of superior π -conjugated charge transfer mediators.

Experimental

Inner-sphere reorganisation energies

Inner-sphere reorganisation energies for both hole (λ_h) and electron (λ_e) charge transfer processes were determined, for the reported crystal structure geometry²³ as well as for **NTDT** model systems, by means of the widely-employed four-point method.^{11,29–31} These were calculated as the sum of the reorganisation energies on going from neutral to radical species and vice-versa. As such, the inner-sphere reorganisation energy on progression from neutral to radical was calculated by subtracting the energy of the neutral specie at its equilibrium geometry to that of the neutral at the equilibrium geometry of the radical. Similarly, the inner-sphere reorganisation energy on going from radical to neutral specie was determined as the difference between the energy of the radical at its equilibrium

geometry and the energy of the radical at the equilibrium geometry of the neutral.

The geometry of neutral (restricted) and radical (unrestricted) geometries were optimised (Table SI.1.1-15) utilising B3LYP,³²⁻³⁴ M06-2X,³⁵ M08-SO,³⁶ M08-HX³⁶ as well as ω B97X-D³⁷ density functionals as implemented in Spartan '18 (v. 1.3.0) software.³⁸ We have previously reported on the effect of basis sets on the computed inner-sphere reorganisation energies of small π -conjugated organic systems³⁹ and as a result calculations in this work were performed employing the 6-311G(d) basis set. In all cases, optimised geometries were confirmed by IR analyses, characterised by the absence of imaginary modes which denotes true equilibria minima. For all radical species, $S^2 < 0.76$ which indicates low spin contamination in all cases.^{40,41}

Inner-sphere reorganisation energies were also computed as a function of torsion of the core thiophene rings in the model **NTDT** structure using the above-mentioned density functionals and basis set. To do this, the torsion of the dihedral angles (θ_1 and θ_2 , Figure 1) formed between the thiophene rings and the **NTDT** core were constrained from 0 to 180°, in 10° increments, for both $\theta_1 = \theta_2$ (asymmetrical) and $\theta_1 = -\theta_2$ (symmetrical).

Two-dimensional model system

A two-dimensional π - π dimer model was generated employing a dimer system formed by two geometry optimised **NTDT** centrosymmetric monomers, whereby the top monomer is simultaneously displaced in 0.30 Å increments over a distance of 16.20 and 12.00 Å along the long and short molecular axes respectively, from a fully eclipsed dimeric geometry as illustrated in Figure 2.

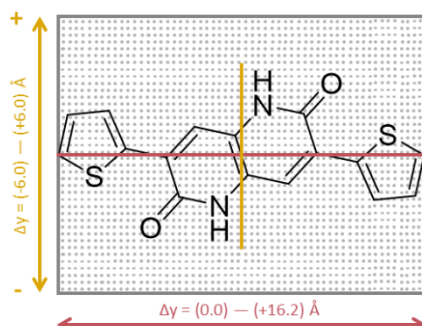


Figure 2. Illustration of the long, Δx (red) and short, Δy (yellow) intermonomer displacements in the generated two-dimensional **NTDT** dimer model system. Grey dots illustrate the location of the reference carbon atom within the thiophene core ring in each of the single point calculations through the x/y map.

This generates a model system with a density of ca 12 single point calculations per Å², which would allow to map the π - π dimer pairs of any crystal structure geometry of **NTDT** based systems. The geometries of the **NTDT** monomers were optimised using M06-2X density functional at the 6-311G(d) level. The relative intermonomer displacement along the vertical axis (Δz) was optimised. To do that, the intermolecular interaction of the fully eclipsed **NTDT** dimer pair was computed first from 3.00 to 5.00 Å on 0.10 Å stepwise and subsequently from 3.65 to 3.75 Å on 0.01 Å stepwise, to localise the energy minimum at 3.74 Å (Figure SI.2.1).

Charge transfer integrals

To evaluate the electronic coupling in these systems, transfer integrals for both hole (t_h) and electron (t_e) transfer processes were determined for the slipped co-facial π - π dimer pair of the reported **NTDT**-based crystal structure²³ as well as dimer pairs of the above explained model system, employing the energy splitting in dimer method.^{11,31} Within the framework of this method, t_h and t_e can be equated to half the splitting between the HOMO/HOMO(-1) and LUMO/LUMO(+1) supramolecular orbitals respectively. Charge transfer integrals were computed employing M06-2X,³⁵ M08-SO,³⁶ M08-HX³⁶ as well as ω B97X-D³⁷ as implemented in Spartan '18 (v. 1.3.0) software.³⁸ To further evaluate the effect of diffusion and polarizability terms in the basis sets, computed $t_{h/e}$ employing our flagship density functional, M06-2X were re-computed using the following basis sets: 6-31G(d), 6-311G(d), 6-311G(d)(p), 6-311+G(d), 6-311++G(d) and 6-311++G(d)(p).

Charge carrier mobilities

Charge carrier mobilities for hole transport (μ_h) along the π - π stacking motif of the reported **NTDT**-based material was calculated by means of the Einstein-Smoluchowski Equation³¹ at T = 298 K:

$$\mu = \frac{1}{2} \frac{e d^2 k_{CT}}{k_B T}$$

where e is the elementary charge, d is the stacking length taken from the crystal structure, k_B is the Boltzmann constant and T is the temperature. k_{CT} is the rate constant for charge transport which can be estimated using the Marcus formalism for charge transfer processes in the high temperature hopping regime:²⁶⁻²⁸

$$k_{CT} = \frac{V^2}{\hbar} \cdot \sqrt{\frac{\pi}{\lambda k_B T}} \cdot \exp\left(-\frac{\lambda}{4k_B T}\right)$$

where \hbar is the reduced Planck constant, λ is the reorganisation energy and V is the electronic coupling or transfer integral (t).

Intermolecular interactions

Intermolecular interactions (ΔE_{CP}) were computed for the reported crystal structure as well as for all dimer pairs in the dimeric **NTDT** model system. In all cases, these were corrected for Basis Set Superposition Error (BSSE) by means of the counterpoise method of Boys and Bernardi.⁴² Similarly to the case of charge transfer integrals, the effect of density functional/basis set on the computed intermolecular interactions was evaluated.

Results and discussion

Inner-sphere reorganisation energies

Inner-sphere reorganisation energies were first computed for the parent **NTDT** system and the effect of density functionals evaluated. To do that, we compare our previously employed density functional, M06-2X to other commonly used ones such as B3LYP and ω B97X-D as well as to more recent versions within Truhlar's toolbox of density functionals, namely M08-HX and M08-SO.

Table 1. Computed $\lambda_{h/e}$ (kJ mol⁻¹) and sum of the changes in bond length throughout the NTDT core motif upon charge transfer, $\Sigma\Delta_{BL}$ (Å) for NTDT optimised geometries using different density functionals (DF) at the 6-311G(d) level.

DF	λ_h	λ_e	$\Sigma\Delta_{BL}(h)$	$\Sigma\Delta_{BL}(e)$
B3LYP	23.3	26.6	0.152	0.242
M08-HX	35.4	39.5	0.206	0.291
M06-2X	35.8	39.5	0.208	0.296
M08-SO	37.0	40.2	0.211	0.301
wB97X-D	41.6	45.5	0.218	0.303

Table 1 summarises the computed $\lambda_{h/e}$ for NTDT optimised geometries utilising different density functionals. It is noteworthy that irrespective of the density functional utilised, we observed that $\lambda_e > \lambda_h$ in all cases. The latter contrasts with values reported for their five-member ring bis-lactam analogue, for which $\lambda_h = 45.6$ kJ mol⁻¹ and $\lambda_e = 21.5$ kJ mol⁻¹ were computed using the same density functional (M06-2X) and a double instead of triple-zeta basis set.³⁹ The effect of density functionals was comprehensively evaluated by means of the added amount of % Hartree-Fock (%HF) (Table 1). We report larger values for both λ_h and λ_e as the amount of %HF exchange implemented in the density functional increases.³²⁻³⁷ In the case of wB97X-D density functional, we ascribe the observed largest values in our dataset to its long range (100%) %HF exchange rather than to its short range (20%),³⁷ which is the same as that implemented in B3LYP density functional.³²⁻³⁴

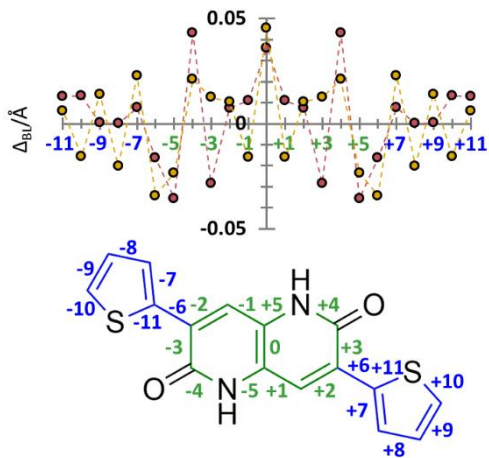


Figure 3. Computed Δ_{BL} on progression from neutral to radical cation (yellow) and anion (red) optimised geometries of NTDT for each chemical bond in the core motif (green) and peripheral core rings (blue).

In light of these findings and to aid in further comparison with previous reports, in the following we will examine in detail computed values employing Truhlar's M06-2X density functional,³⁵ with comparable trends observed for other density functionals (Figure SI.3.1-5).

Changes in bond lengths, Δ_{BL} throughout the model NTDT core motif (green) and core thiophene rings (blue) were measured for relaxed geometries and plotted against their bond numbers (Figure 3). Δ_{BL} were computed by subtracting the bond length of a given bond in the radical geometry from the bond length in the neutral specie for the same chemical bond. As such, positive (negative) changes are consistent with an elongation (shortening) of the chemical bond on

going from neutral to radical relaxed geometries. Irrespective of the charge transfer process, we report that chemical bonds exhibiting larger variations are primarily located within the core of the NTDT system and that the sum of these changes can further account for the computed $\lambda_{h/e}$ (Table 1). The latter would suggest that unlike those observations made for phenyl torsion in its five-member ring analogue,³⁹ the torsion of the core rings on 1,5-naphthyridines has lower impact on the inner-sphere reorganisation energies. In fact, if Δ_{BL} within the core rings are considered, bond length changes do not account for the computed inner-sphere reorganisation energies. The latter is particularly relevant if the design employs peripheral substitutions that result in larger dihedral angles of the core rings with respect to the core motif.¹⁴

Judicious evaluation of the findings illustrated in Figure 3 reveal that the effect of charge transfer on Δ_{BL} is critically influenced by the single/double bond nature of chemical bonds in the neutral form, with greater distinction between electron/hole processes often observed in single bonds. As such, whilst the decrease in double bond character of bonds 0 and +/-2 occurs to a similar extent in the case of hole and electron transfer processes, the increase in single bond character of chemical bonds +/-4 is significantly greater upon addition of an electron. Of particular note is the behaviour of chemical bonds +/-1 and +/-3, which contrary to previous observations, are characterised by bond elongation/shortening on progression to relaxed radical geometries which depend on the nature of the charge transfer process. In this regard, we compute that chemical bonds +/-1 are elongated upon addition of an electron and in turn shortened when an electron is taken out ($d = 1.375, 1.359$ and 1.386 in the relaxed neutral, radical cation and radical anion geometries, respectively). The opposite behaviour is observed for chemical bonds +/-3, with measured $\Delta_{BL} > 0$, consistent with chemical bond elongation on progression to the radical cation geometry ($d = 1.480, 1.493$ and 1.452 in the relaxed neutral, radical cation and radical anion geometries, respectively). Via careful analysis of these structural re-arrangements, we ascribe them, and the observed trends in computed $\lambda_{h/e}$, to the alleviation of the intramolecular repulsive interaction between the electronegative thiophene sulfur atoms and the electronegative carbonyl oxygens, which is enhanced upon addition of an electron in the formation of the radical anion. Structurally, the latter can be observed in the changes to intramolecular distances between these two atoms ($d_{S-O} = 2.740, 2.735$ and 2.750 Å in the relaxed geometries of neutral, radical cation and radical anion, respectively).

To further understand the structural implications of radical formation and the potentially low impact of ring torsion previously anticipated, we deemed appropriate to evaluate the effect of this structural re-arrangement on computed $\lambda_{h/e}$. To do that, both core rings were twisted simultaneously from $\theta = 0 - 180^\circ$ on 10° stepwise. We observed that simultaneous symmetrical ($\theta_1 = -\theta_2$) and asymmetrical ($\theta_1 = \theta_2$) torsion of both thiophene rings as well as results obtained for other density functionals conform to the same trends (Figure SI.4.1-10). In the following, we will focus on the results obtained for the symmetrical torsion employing M06-2X density functional.

In agreement with our previous observation for optimised geometries, it is striking to us the significantly lower impact of core ring torsion ($\Delta\lambda_{h/e} (\theta = 0-90^\circ) = 1.25/18.59$ kJ mol⁻¹) when compared to

phenyl-substituted diketopyrrolopyrroles.³⁹ Upon detailed observation of the frontier molecular orbitals (Figure 1), we partially ascribe these findings to the bonding/anti-bonding character of the chemical bond linking the naphthyridine core to the thiophene rings (bond +/-6, Figure 3). The latter switches from anti-bonding character in the HOMO to bonding in the LUMO, hence the larger sensitivity of λ_e towards core ring torsion due to the disruption of the bonding nature in the latter upon torsion.

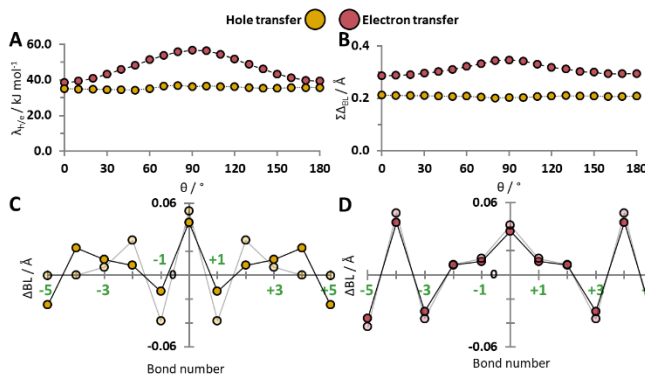


Figure 4. Computed $\lambda_{h/e}$ (A) and sum of changes in bond length in the NTDT core motif (B) as a function of simultaneous torsion of the core rings ($\theta_1 = -\theta_2$). Computed Δ_{BL} on progression from neutral to radical cation (C) and anion (D) geometries of NTDT for each chemical bond in the NTDT core (solid/transparent filled circles denote geometries at $\theta_1 = -\theta_2 = 0$ and 90° respectively).

Similarly to the observations made for the unconstrained geometries, changes in bond lengths within the core motif and not throughout the model NTDT structure upon charge transfer exhibit positive correlations with computed $\lambda_{h/e}$. The increase in λ_e as the thiophene rings are twisted can be attributed to increasingly larger Δ_{BL} across all chemical bonds in the core motif (Figure 4D). In turn, we observed negligible impact of ring torsion on computed λ_h . In this regard, whilst Δ_{BL} increases as the rings are twisted for chemical bonds 0, +/-1 and +/-2 when taking an electron out to generate the radical cation, the remaining bonds in the core motif exhibit opposite behaviour (Figure 4C). In fact, the Δ_{BL} for these other chemical bonds at the planar (0 and 180° , solid filled circles in Figure 4C) geometries are greater than those observed at 90° (transparent filled circles in Figure 4C), hence counteracting the variations described for the other chemical bonds within the NTDT core motif. The latter is particularly notorious in the case of chemical bonds +/-4 and +/-5. Whilst the single bonded nature of bonds +/-4 is enhanced upon generation of the radical cation, bonds +/-5 are characterised by $\Delta_{BL} < 0 \text{ \AA}$ for planar geometries. However, and contrary to the situation observed for electron transfer processes, bond lengths of bonds +/-4 and +/-5 for twisted ($\theta = 90^\circ$) geometries exhibit negligible differences between the neutral and radical cation forms ($d_{+/-4//+/-5} = 1.367/1.390//1.417/1.392 \text{ \AA}$ and $1.356/1.356//1.428/1.427 \text{ \AA}$ for the constrained neutral/radical cation at $\theta = 0$ and 90° , respectively). Subsequently, we went on to determine the inner-sphere reorganisation energies of relaxed NTDT-based geometries, including the only reported crystal structure of a substituted 1,5-naphthyridine.²³ The generated model for the torsion of the core rings was observed to account well for the computed $\lambda_{h/e}$ for relaxed geometries of NTDT system ($\lambda_{h/e} = 35.8/39.5$ and $35.1/38.5 \text{ kJ mol}^{-1}$ for the fully relaxed NTDT with $\theta = 1.13^\circ$ and the model NTDT

geometry constrained for $\theta = 0.00^\circ$, respectively) as well as optimised reported crystal structure ($\lambda_{h/e} = 37.6/43.9$ and $34.7/41.1 \text{ kJ mol}^{-1}$ for the optimised crystal structure with $\theta = 18.82^\circ$ and the NTDT geometry constrained for $\theta = 20.00^\circ$, respectively). The latter supports our observations that λ_e exhibits a greater sensitivity to core ring torsion than λ_h does. In addition, these calculations on unconstrained geometries serve to ratify the ability of our developed model in accounting for $\lambda_{h/e}$ in a broader range of N-substituted derivatives.

Charge transfer integrals

Firstly, the effect of different basis sets and density functionals on computed $t_{h/e}$ was evaluated by a one-dimensional NTDT dimer model system whereby both monomers in the dimer pair are fully eclipsed and the top monomer is then displaced with respect to the bottom one along the NTDT long (x) molecular axis (Figure 2 for $\Delta x = 0.00 \text{ \AA}$). For the widely employed M06-2X density functional,^{7,10,35} we report that progression from double to triple zeta basis set as well as the addition of polarisability and diffusion functions result in very small effects on the computed charge transfer integrals as summarised in Table 2 for the NTDT dimer pair at $\Delta x/y/z = 3.30/0.00/3.74 \text{ \AA}$. Similarly, and in agreement with previous results,^{10,35-37} negligible differences in $t_{h/e}$ were observed for all the density functionals as investigated at the 6-311G(d) level as summarised in Table 2 for the NTDT dimer pair at $\Delta x/y/z = 3.30/0.00/3.74 \text{ \AA}$.

Table 2. Computed hole (t_h) and electron (t_e) transfer integrals and intermolecular interactions (ΔE_{CP}) in kJ/mol for the NTDT dimer pair at $\Delta x/y/z = 3.30/0.00/3.74 \text{ \AA}$ as a function of basis sets, employing the M06-2X density functional (Figure S1.5.1, S1.5.2 and S1.9.1 for t_h , t_e and ΔE_{CP} , respectively) and for different density functionals (DF) at the 6-311G(d) level (Figure S1.5.1, S1.5.2 and S1.9.1 for t_h , t_e and ΔE_{CP} , respectively).

M06-2X/Basis set	t_h	t_e	ΔE_{CP}
6-31G(d)	4.34	5.79	-42.7
6-311G(d)	4.82	5.79	-56.5
6-311G(d)(p)	4.82	5.79	-56.0
6-311+G(d)	5.79	7.72	-56.8
6-311++G(d)	5.79	7.72	-56.7
6-311++G(d)(p)	4.34	5.31	-56.8
DF/6-311G(d)			
M08-HX	4.34	5.79	-54.0
M06-2X	4.82	5.79	-56.5
M08-SO	4.34	5.79	-57.2
wB97X-D	4.34	5.79	-73.4

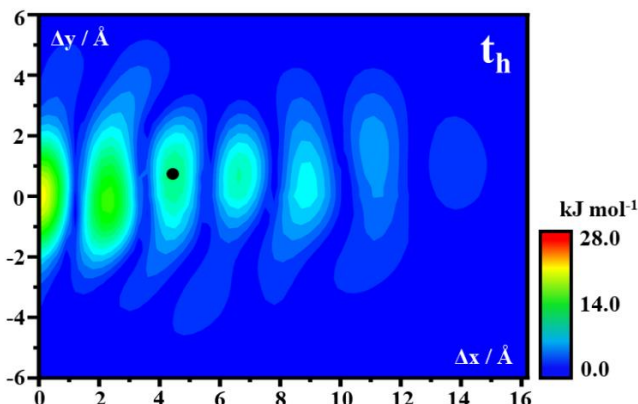


Figure 5. Three-dimensional map of the computed hole transfer integrals as a function of the simultaneous displacements along the long (x) and short (y) molecular axes in a **NTDT** dimer model system. M06-2X/6-311G(d). Black solid circle illustrates the location of the reported crystal structure ($\Delta x/y = 4.39/0.79 \text{ \AA}$).

As a result, and for ease of comparison with previous studies,^{7,9,10} in the following M06-2X density functional and 6-311G(d) basis set are utilised. Charge transfer integrals were calculated for dimer pairs of the parent **NTDT** system by simultaneously displacing the top monomer with respect to the bottom one along their long (x) and short (y) molecular axes, resulting in a two-dimensional model system. Figure 5 illustrates the effect of $\Delta x/\Delta y$ on computed hole transfer integrals in NTDT-based systems. In both cases, a number of regions of local maxima/minima are identified, which are consistent with the nodal progression in the wavefunction of the frontier molecular orbitals (Figure 1). It is noteworthy that contrary to the symmetry observed in phenyl substituted analogues, systems whereby thiophene rings are employed as core rings are asymmetric with respect to their long molecular axis (Figure 2). As a result, asymmetry is observed in both frontier molecular orbitals (Figure 1). In the case of t_h , computed values as a function of Δx take the form of damped oscillations with maxima located at ca 0.00, 2.40, 4.50, 6.60, 8.70, 11.10 and 13.80 \AA . Although the overlap between the HOMO surfaces of the monomers decreases as these are displaced with respect to one another, NTDT-based dimer pairs exhibiting relatively large Δy should not be discarded solely on those bases. In fact, we report large computed t_h for Δy values greater than 2.00 \AA (e.g. $t_h = 7.5 \text{ kJ mol}^{-1}$ for $\Delta x/y = 2.40/-2.10 \text{ \AA}$). Interestingly, the described damped oscillations described for long molecular axis displacements at $\Delta y = 0.00 \text{ \AA}$, exhibit a different pattern for $\Delta y > 2.40 \text{ \AA}$, albeit with negligible differences in the location of the local maxima, whereby the largest t_h values are computed for $\Delta x = 3.00$ and 11.10 \AA instead of $\Delta x = 0.00$ and 2.40 \AA observed for $\Delta y = 0.00 \text{ \AA}$ long axis displacements (Figure 5). Along these lines it is of note that the latter was not observed for positive displacements along the short molecular axis, which we ascribed to the above-mentioned asymmetry in the HOMO surface.

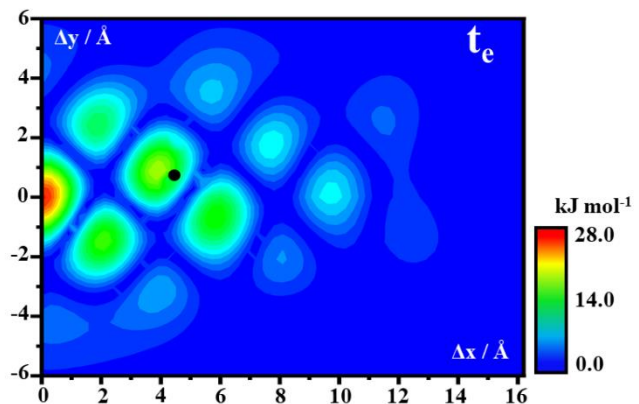


Figure 6. Three-dimensional map of the computed electron transfer integrals as a function of the simultaneous displacements along the long (x) and short (y) molecular axes in a **NTDT** dimer model system. M06-2X/6-311G(d). Black solid circle illustrates the location of the reported crystal structure ($\Delta x/y = 4.39/0.79 \text{ \AA}$).

We observed that the computed electron transfer integral for the fully eclipsed **NTDT** dimer ($\Delta x = \Delta y = 0.00 \text{ \AA}$) exceeds that computed for the hole transfer process ($t_{h/e} = 21.4/27.4 \text{ kJ mol}^{-1}$). Interestingly, intermonomer displacements along the long molecular axis ($\Delta y = 0.00 \text{ \AA}$) do not conform to the damped oscillations observed for t_h (Figure 5-6). As such, local maxima located at ca $\Delta x = 2.10 \text{ \AA}$ is denoted by a small splitting of the supramolecular orbitals ($t_e = 2.4 \text{ kJ mol}^{-1}$). In turn, large t_e are computed for dimer pairs for maxima located at ca $\Delta x = 3.90$ and 6.00 \AA ($t_e = 11.5$ and 12.0 kJ mol^{-1} at $\Delta x = 3.90$ and 6.00 \AA , respectively). Along those lines, it is also of note that large t_e values are not solely limited to dimer pairs which are closely aligned along the short molecular axis (Figure 2). The latter, which can be associated to the LUMO surface of **NTDT** systems, facilitates the realisation of dimer pairs characterised by large LUMO-LUMO(+1) splitting despite their significant short molecular axis shifts (e.g. $t_e = 7.7$ and 5.8 kJ mol^{-1} for NTDT dimer pairs at $\Delta x/y = 7.80/-1.80$ and $5.70/-3.60 \text{ \AA}$, respectively). The latter contrasts with the popular misconception that small intermonomer Δy are essential in π -stacking supramolecular architectures in order to develop successful charge mediating materials.

Next, it was of interest to evaluate in detail the observed reversal of the charge transfer character of NTDTs for small (ca 1.00 \AA) intermonomer displacements. For example, a 1.20 \AA shift along the long molecular axis from $\Delta x = 2.40$ to 3.60 \AA ($\Delta y = 0.00 \text{ \AA}$) is responsible for the complete reversal of the $t_{h/e}$ character in these systems. As illustrated in Figure 7, the HOMO at 2.40 \AA is gerade and exhibits strong anti-bonding character. In turn, the ungerade HOMO(-1) is characterised by strong wavefunction overlap, hence resulting in a large computed transfer integral ($t_h = 15.3 \text{ kJ mol}^{-1}$). By displacing the top monomer with respect to the bottom one by 1.20 \AA , the HOMO lowers its energy to become the HOMO(-1), changing its symmetry to ungerade and exhibiting a weakly bonding character at $\Delta x = 3.60 \text{ \AA}$. Analogously, the energy of the HOMO(-1) at $\Delta x = 2.40 \text{ \AA}$ increases and becomes the HOMO with a gerade symmetry and a weakly anti-bonding nature, hence lowering the computed integral ($t_h = 2.1 \text{ kJ mol}^{-1}$). Similarly, the small intermonomer displacement results in the reversal of the weakly bonding/anti-bonding character of the LUMO/LUMO(+1) to a strong bonding/ant-bonding respectively, with the associated increase in computed electron

transfer integral ($t_e = 1.3$ and 11.3 kJ mol^{-1} for the **NTDT** dimer pair at $\Delta x = 2.40$ and 3.60 \AA , respectively). However, the potential ability to thermally induce such changes is greatly determined by the strength of the intermolecular interactions between neighbouring monomers within the supramolecular motifs. As a result, we will devote the last part of this work to the in-depth understanding of intermolecular interactions in **NTDT**-based materials.

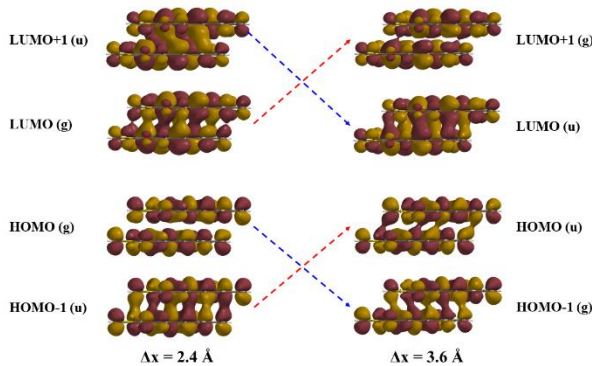


Figure 7. Illustration of the computed Kohm-Sham supramolecular orbitals of **NTDT** dimer model systems displaced at $\Delta x = 2.40$ (left) and 3.60 (right) \AA ($\Delta y = 0.00 \text{ \AA}$). M06-2X/6-311G(d). IsoVal = 0.01.

In testing our developed two-dimensional model system, we went on to compute the charge transfer integral for the slipped cofacial π - π dimer pair of the reported crystal structure ($\Delta x/y/z = 4.39/0.79/3.50 \text{ \AA}$, Figure 1), resulting in $t_{h/e} = 13.1/1.8 \text{ kJ mol}^{-1}$. In this regard, it is of note that there are other four nearest neighbouring dimer pairs in addition to this π - π dimer pair, for which transfer integrals were also computed (Table SI.7.1). In particular, and in agreement with previous reports, we highlight the stacking motif propagating along the c crystallographic axis, for which we compute $t_{h/e} = 3.2/1.8 \text{ kJ mol}^{-1}$. Whilst these are lower than the computed values for the π - π dimer pair, the appearance of more than one charge propagating channel in organic charge transfer mediators plays an important role in circumventing problems associated to defects and impurities and is beneficial to the overall performance.¹

In relation to the π - π dimer pair, we further computed $t_{h/e} = 7.5/1.9 \text{ kJ mol}^{-1}$ for the **NTDT** model dimer pair characterised by such intermonomer displacements along the long and short molecular axis ($\Delta z = 3.74 \text{ \AA}$). It is striking that our model system was able to predict the relative order of charge transfer nature (i.e. $t_h > t_e$) and to further provide a qualitative measurement in line with the computed values for the N-substituted material. In light of the observed negligible impact of N-alkyl groups on wavefunction localisation for both frontier molecular orbitals, we ascribed these differences to variations in Δz (vide supra). Importantly, these findings highlight that, irrespective of the N-substitution, the reported model system can be employed in the determination of charge transfer integrals by solely knowing the intermonomer displacements in the supramolecular crystal arrangements. In addition, these results provide an example that highlights the importance of i) the asymmetry with respect to the long molecular axis in **NTDT** based systems as well as ii) the impact of small displacements on $t_{h/e}$, previously observed for other systems.^{9,10,21} In this regard, we compute critically different charge transfer properties for the dimer pair exhibiting negative instead of positive displacement along the

short molecular axis ($\Delta y = -0.79 \text{ \AA}$). Contrary to the hole transfer character of the previously described one ($t_{h/e} = 7.5/1.9 \text{ kJ mol}^{-1}$ for the dimer pair at $\Delta x/y = 4.39/0.79 \text{ \AA}$), we compute a decrease in t_h and a striking increase in t_e as a result of the ca 1.58 \AA short axis shift from $\Delta y = 0.79$ to -0.79 \AA ($t_{h/e} = 10.6/14.9 \text{ kJ mol}^{-1}$ for the dimer pair at $\Delta x/y = 4.39/-0.79 \text{ \AA}$).

On comparing the large t_h with other small organic systems, we report the computed value to be larger than that obtained for the slipped-cofacial π - π dimer pair of orthorhombic rubrene^{9,10} and amongst the highest computed for diketopyrrolopyrrole-based materials.¹⁰ Subsequently, utilising the crystallographic unit cell length along which the one-dimensional stacking motif propagates (d_b axis = 5.67 \AA) and our computed $\lambda_h = 37.6 \text{ kJ mol}^{-1}$ and $t_h = 13.1 \text{ kJ mol}^{-1}$ we estimate hole mobility of ca $1.46 \text{ cm}^2 \text{ V}^{-1} \text{ s}^{-1}$, which remarkably agrees with hole mobilities experimentally measured in thin film devices ($\mu_h = 1.29 \text{ cm}^2 \text{ V}^{-1} \text{ s}^{-1}$) and in vacuum-processed and spin-coated devices ($\mu_h = 1.10 \text{ cm}^2 \text{ V}^{-1} \text{ s}^{-1}$).²⁴ These results further warrant the development of novel materials exploiting naphthyridine chemistries towards their application as charge transfer mediators in optoelectronic applications.

Intermolecular interactions

In light of the observed impact of small intermonomer displacements on the transfer integrals nature, we devote the remainder of the manuscript to the in-depth analysis of intermolecular interactions (ΔE_{CP}) in **NTDT** based systems. First, the effect of basis sets and density functionals on computed ΔE_{CP} was evaluated by means of one-dimensional dimer model systems ($\Delta y/z = 0.00/3.74 \text{ \AA}$). Comparable trends were observed for all density functionals, with the larger absolute values computed for wB97X-D, as summarised in Table 2 (Figure SI.8.1). In relation to the results obtained for different basis sets, it is of note that our findings support negligible improvements for basis sets larger than 6-311G(d) despite their significantly greater computational cost (Table 2 and Figure SI.9.1).

We then computed ΔE_{CP} for the slipped cofacial π - π dimer pair of the reported crystal structure. The large ($\Delta E_{CP} = -86.8 \text{ kJ mol}^{-1}$) computed intermolecular interaction was observed to be larger than those computed for most DPP-based systems¹⁰ and further represent a dramatic increase with respect to $\Delta E_{CP} = -35.6 \text{ kJ mol}^{-1}$ computed for orthorhombic rubrene's π - π dimer pair.^{9,10} Intermolecular interactions were also computed for all nearest neighbouring dimer pairs of the reported system (Table SI. 7.1). We report significantly lower intermolecular interactions for these dimer pairs when compared to the π - π dimer pair, with the ΔE_{CP} of the alternative charge propagation channel compromising its thermal integrity and indicating that the overall supramolecular structures is critically determined by the π - π stacking motif.

Contrary to the minimal impact of the N-substitution on computed transfer integrals, removal of the side chains results in lowering the computed intermolecular interaction by 19.1 kJ mol^{-1} ($\Delta E_{CP} = -67.1 \text{ kJ mol}^{-1}$ for the dimer pair with removed alkyl chains), which we ascribe to stabilising interchain interactions but more importantly to intermolecular attractive interactions between electronegative carbonyl oxygen atoms and electropositive hydrogen atoms within the side chains located 2.439 \AA apart (Figure 8).

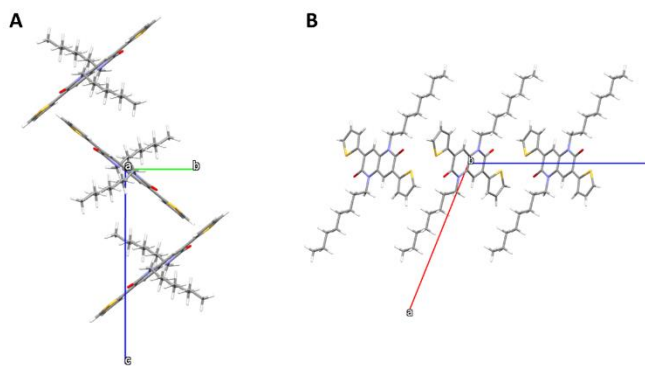


Figure 8. Capped-stick illustration of nearest neighbouring interactions in the crystal lattice of the reported NTD-based system viewed along the a (left) and b (right) crystallographic axes. Reference monomer located at (0,0,0).

Along those lines, it was of surprise to us that contrary to chemical intuition, the relative orientation of the core thiophene rings where intramolecular O--H and S--H are not favoured. In turn, the orientation of the core rings results in relatively close distance between thiophene sulphur and carbonyl oxygen atoms at 2.685 Å. We ascribed the latter to intermolecular interactions of the thiophene rings with side alkyl chains and thiophene rings of monomers located at (0,1/2,1/2) and (0,-1/2,-1/2) with respect to the monomer at (0,0,0), which are not part of the one-dimensional stacking motif (Figure 8).

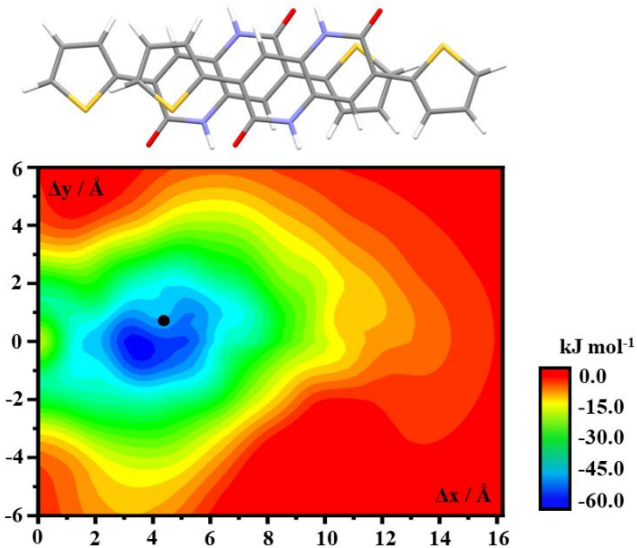


Figure 9. Illustration of the supramolecular geometry of the NTD dimer pair at global minimum of the model system (top). Three-dimensional map illustrating the computed intermolecular interactions as a function of simultaneous intermonomer displacements along the long and short molecular axes in a NTD dimer model system. M06-2X/6-311G(d) (bottom). Black solid circle illustrates the location of the reported crystal structure ($\Delta x/y = 4.39/0.79 \text{ \AA}$).

These observations and the large thermal integrity calculated for the slipped cofacial dimer pair in the crystal structure, motivated us to determine the impact of intermonomer displacements on the computed dimer binding energies. Figure 9 illustrates these effects as a function of simultaneous long and short molecular axes displacements in a model NTD dimer system. The three-dimensional potential energy surface is characterised by multiple

local minima located at ca $\Delta x = 1.50, 3.30, 4.80, 7.20$ and 13.20 \AA for $\Delta y = 0.00 \text{ \AA}$, with an identified global minimum at $\Delta x/y = 3.30/0.00 \text{ \AA}$ ($\Delta E_{CP} = -54.3 \text{ kJ mol}^{-1}$). It is of note that the model system was observed to account well for the intermonomer displacements in the π - π dimer pair of the reported crystal structure. Comparably strong intermolecular interactions to those of the dimer pair at the global minimum were also computed for dimer pairs with their greater Δy (e.g. $\Delta E_{CP} = -50.4 \text{ kJ mol}^{-1}$ for dimer pair at $\Delta x/y = 3.60$ and 0.90 \AA), which are often neglected. In addition, we report large ($\Delta E_{CP} < -45.0 \text{ kJ mol}^{-1}$) for dimer pairs in the two-dimensional model system characterised by $3.30 \text{ \AA} < \Delta x < 5.40 \text{ \AA}$ and $-0.60 \text{ \AA} < \Delta y < 0.90 \text{ \AA}$. We observe that, irrespective of the displacements along the short molecular axis, the Δx location of the global minimum remains unaltered. We attribute the geometry of the NTD dimer pair at the global minimum to the synergistic effect of favourable bond dipole and induced bond dipole interaction that further dictate the location of the local minima. In particular, we highlight the electrostatic intermolecular interaction between electropositive carbonyl carbon atoms in one monomer and electronegative sulfur atoms of the other monomer in the dimer pair, which are maximised at this supramolecular geometry (Figure 9). In turn, we associate the weaker local minima at $\Delta x = 4.8 \text{ \AA}$ ($\Delta E_{CP} = -50.8 \text{ kJ mol}^{-1}$ at $\Delta y = 0.0 \text{ \AA}$), which closely coincides with the Δx in the reported crystal structure, to the intermolecular interaction between electronegative sulfur atoms of one monomer and transannular bond carbon atoms of the other monomer in the dimer pair which are less electropositive than the carbonyl carbon atoms.

Conclusions

In this work we report an in-depth systematic evaluation of the charge transfer behavior of thiophene substituted naphthyridine materials utilising a series of bespoke model systems. Larger electron than hole inner-sphere reorganization energies were computed in all cases and irrespective of thiophene rings torsion with respect to the NTD core. Interestingly, λ_h exhibited negligible sensitivity with respect to the core rings torsion, which we ascribed to counteracting structural re-arrangements within the core. Via judicious analysis of those structural ‘motions’ upon radical generation we associate computed $\lambda_{h/e}$ to Δ_{BL} within the NTD core and not the peripheral thiophene rings. Both, transfer integrals and dimeric intermolecular interactions were studied thoroughly by means of two-dimensional model systems. In both cases, we report asymmetrical three-dimensional PES with respect to the long molecular axis of the model system. Large $t_{h/e}$ were computed even for dimer pairs characterised by large short axis displacements, which are often believed to be associated to poor performance and as a result ruled out from experimental evaluations. In addition, these supramolecular geometries were computed to exhibit strong intermolecular interactions that confer them with highly desirable thermal integrities. The latter becomes particularly relevant in light of the observed sensitivity of $t_{h/e}$ to small intermonomer displacements. In relation to the effect of density functionals and basis sets on those computed charge transfer properties, our results are consistent with similar trends in computed $\lambda_{h/e}$ irrespective of the density functional utilised and increasingly large $|\lambda_{h/e}|$ were computed as the %HF

exchange in the functional increases. Whilst we report negligible impact of density functional/basis set on the computed t_{he} , ΔE_{CP} obtained by means of ω B97X-D were observed to be significantly larger than those computed for the other investigated density functionals. It is of note that increasing the size of the basis sets beyond that of the commonly used 6-311G(d) results in negligible variations in computed ΔE_{CP} despite the associated significant increase in computational cost. The latter represents a valuable information for those materials scientists with limited computational resources. Importantly, our developed model systems were observed to account well for computed properties in reported crystalline materials by simply knowing their crystallographic parameters and to further agree with experimental observations quantitatively. In summary, our results imply that thiophene substituted naphthyridines materials denote a promising superior alternative to currently exploited systems and as a result, we anticipate that this work will motivate materials scientists to efficiently design and engineer superior charge transfer mediators exploiting naphthyridine chemistries.

Conflicts of interest

There are no conflicts to declare.

Acknowledgements

This work was financially supported by the Royal Society of Chemistry [RF19-0974]. JCC acknowledges funding for MML and AAA from the University of Hertfordshire.

Notes and references

- 1 O. Ostroverkhova, *Chemical Reviews*, 2016, **116**, 13279–13412.
- 2 G. Schweicher, Y. Olivier, V. Lemaur and Y. H. Geerts, *Israel Journal of Chemistry*, 2014, **54**, 595–620.
- 3 H. Chung and Y. Diao, *Journal of Materials Chemistry C*, 2016, **4**, 3915–3933.
- 4 M. Schwoerer and C. H. Wolf, *Organic Molecular Solids*, Wiley-VCH, 2007.
- 5 M. E. Gershenson, V. Podzorov and A. F. Morpurgo, *Reviews of Modern Physics*, 2006, **78**, 973–989.
- 6 R. Li, W. Hu, Y. Liu and D. Zhu, *Accounts of Chemical Research*, 2010, **43**, 529–540.
- 7 J. Vura-Weis, M. A. Ratner and M. R. Wasielewski, *Journal of the American Chemical Society*, 2010, **132**, 1738–1739.
- 8 A. Troisi, *Chemical Society Reviews*, 2011, **40**, 2347–2358.
- 9 S. J. Chung, C. J. McHugh and J. Calvo-Castro, *Journal of Materials Chemistry C*, 2019, **7**, 2029–2036.
- 10 J. Calvo-Castro and C. J. McHugh, *Journal of Materials Chemistry C*, 2017, **5**, 3993–3998.
- 11 J. L. Bredas, D. Beljonne, V. Coropceanu and J. Cornil, *Chemical Reviews*, 2004, **104**, 4971–5003.
- 12 J. L. Bredas, J. P. Calbert, D. A. da Silva and J. Cornil, *Proceedings of the National Academy of Sciences of the United States of America*, 2002, **99**, 5804–5809.
- 13 Y. Li, P. Sonar, L. Murphy and W. Hong, *Energy & Environmental Science*, 2013, **6**, 1684–1710.
- 14 J. Calvo-Castro, S. Maczka, C. Thomson, G. Morris, A. R. Kennedy and C. J. McHugh, *CrystEngComm*, 2016, **18**, 9382–9390.
- 15 L.-F. Ji, J.-X. Fan, G.-Y. Qin, N.-X. Zhang, P.-P. Lin and A.-M. Ren, *J. Phys. Chem. C*, 2018, **122**, 21226–21238.
- 16 D. Chandran and K.-S. Lee, *Macromolecular Research*, 2013, **21**, 272–283.
- 17 H. M. Smith, *High Performance Pigments*, Wiley-VCH, 2002.
- 18 W. Herbst and K. Hunger, *Industrial Organic Pigments*, Wiley-VCH, 2004.
- 19 J. Calvo-Castro, G. Morris, A. R. Kennedy and C. J. McHugh, *Crystal Growth & Design*, 2016, **16**, 2371–2384.
- 20 J. Calvo-Castro, G. Morris, A. R. Kennedy and C. J. McHugh, *Crystal Growth & Design*, 2016, **16**, 5385–5393.
- 21 J. Calvo-Castro, M. Warzecha, A. R. Kennedy, C. J. McHugh and A. J. McLean, *Crystal Growth & Design*, 2014, **14**, 4849–4858.
- 22 J. Calvo-Castro, M. Warzecha, I. D. H. Oswald, A. R. Kennedy, G. Morris, A. J. McLean and C. J. McHugh, *Crystal Growth & Design*, 2016, **16**, 1531–1542.
- 23 W. S. Yoon, D. W. Kim, J.-M. Park, I. Cho, O. K. Kwon, D. R. Whang, J. H. Kim, J.-H. Park and S. Y. Park, *Macromolecules*, 2016, **49**, 8489–8497.
- 24 J. H. Kim, M.-W. Choi, W. S. Yoon, S. Oh, S. H. Hong and S. Y. Park, *ACS Applied Materials and Interfaces*, 2019, **11**, 8301–8309.
- 25 B. Frydman, M. Los and H. Rapoport, *J. Org. Chem.*, 1971, **36**, 450–454.
- 26 R. A. Marcus, *Reviews of Modern Physics*, 1993, **65**, 599–610.
- 27 R. A. Marcus and N. Sutin, *Biochimica Et Biophysica Acta*, 1985, **811**, 265–322.
- 28 M. Bixon and J. Jortner, in *Electron Transfer-from Isolated Molecules to Biomolecules, Pt 1*, eds. J. Jortner and M. Bixon, 1999, vol. 106, pp. 35–202.
- 29 S. F. Nelsen, S. C. Blackstock and Y. Kim, *Journal of the American Chemical Society*, 1987, **109**, 677–682.
- 30 V. Coropceanu, M. Malagoli, D. A. da Silva, N. E. Gruhn, T. G. Bill and J. L. Bredas, *Physical Review Letters*, 2002, **89**, 2755031–2755034.
- 31 V. Coropceanu, J. Cornil, D. A. da Silva Filho, Y. Olivier, R. Silbey and J.-L. Bredas, *Chemical Reviews*, 2007, **107**, 926–952.
- 32 A. D. Becke, *Journal of Chemical Physics*, 1993, **98**, 5648–5652.
- 33 C. T. Lee, W. T. Yang and R. G. Parr, *Physical Review B*, 1988, **37**, 785–789.
- 34 A. D. Becke, *Physical Review A*, 1988, **38**, 3098–3100.
- 35 Y. Zhao and D. G. Truhlar, *Theoretical Chemistry Accounts*, 2008, **120**, 215–241.
- 36 Y. Zhao and D. G. Truhlar, *J. Chem. Theory Comput.*, 2008, **4**, 1849–1868.
- 37 J.-D. Chai and M. Head-Gordon, *Physical Chemistry Chemical Physics*, 2008, **10**, 6615–6620.
- 38 Y. Shao, L. F. Molnar, Y. Jung, J. Kussmann, C. Ochsenfeld, S. T. Brown, A. T. B. Gilbert, L. V. Slipchenko, S. V. Levchenko, D. P. O'Neill, R. A. DiStasio Jr., R. C. Lochan, T. Wang, G. J. O. Beran, N. A. Besley, J. M. Herbert, C. Y. Lin, T. Van Voorhis, S. H. Chien, A. Sodt, R. P. Steele, V. A. Rassolov, P. E. Maslen, P. P. Korambath, R. D. Adamson, B. Austin, J. Baker, E. F. C. Byrd, H. Dachsel, R. J. Doerksen, A. Dreuw, B. D. Dunietz, A. D. Dutoi, T. R. Furlani, S. R. Gwaltney, A. Heyden, S. Hirata, C.-P. Hsu, G. Kedziora, R. Z. Khaliulin, P. Klunzinger, A. M. Lee, M. S. Lee, W. Liang, I. Lotan, N. Nair, B. Peters, E. I. Proynov, P. A. Pieniazek, Y. M. Rhee, J. Ritchie, E. Rosta, C. D. Sherrill, A. C. Simmonett, J. E. Subotnik, H. L. Woodcock III, W. Zhang, A. T. Bell, A. K. Chakraborty, D. M. Chipman, F. J. Keil, A. Warshel, W. J. Hehre, H. F. Schaefer III, J.

- Kong, A. I. Krylov, P. M. W. Gill and M. Head-Gordon, *Physical Chemistry Chemical Physics*, 2006, **8**, 3172–3191.
- 39 J. Calvo-Castro, C. J. McHugh and A. J. McLean, *Dyes and Pigments*, 2, **113**, 609–617.
- 40 F. Jensen, *Introduction to computational chemistry*, John Wiley and sons, 2007.
- 41 A. Szabo and N. S. Ostlund, *Modern Quantum Chemistry: Introduction to Advanced Electronic Structure Theory*, McGraw-Hill, 1989.
- 42 S. F. Boys and F. Bernardi, *Molecular Physics*, 2002, **100**, 65–73.